Journal of Nanoscience and Nanoengineering
Vol. 4, No. 2, 2018, pp. 9-16
http://www.aiscience.org/journal/jnn
ISSN: 2471-8378 (Print); ISSN: 2471-8394 (Online)

Structural and Dielectric Properties of Mn Doped $BiFeO_3$

Katrapally Vijaya Kumar[1, *], Voora Srinivas[2], Anupati Telugu Raghavender[3, 4]

[1]Department of Physics, JNTUH College of Engineering Sultanpur, Pulkal (M), Sangareddy, India
[2]Department of Physics, Government Institute of Electronics, Secunderabad, India
[3]Department of Electronics and Communication Engineering, Nishitha College of Engineering and Technology, Hyderabad, India
[4]Abhigyaan Labs Private Limited, Hyderabad, India

Abstract

Polycrystalline $Bi_{1-x}Mn_xFeO_3$(x=0.0, 0.1, 0.2, 0.3) were synthesized using sol-gel method to study the structural and dielectrical properties. Raman analysis confirmed the rhombohedral structure (3Rc) in all the prepared samples. Raman measurements were carried in both parallel and crossed polarization configuration. In dielectric studies, dielectric constant (both ε' and ε") and dielectric loss were observed to decrease with increasing frequency (100Hz to 1MHz) at room temperature. Dielectric constant and dielectric loss increases with increases in temperature. Leakage current density was observed to increase with increasing Mn doping concentration.

Keywords

Multiferroic Material, Structural Properties, Dielectric Properties, Leakage Current

Received: April 18, 2018 / Accepted: May 17, 2018 / Published online: June 14, 2018

1. Introduction

Multiferroic materials may be classified as materials in which ferromagnetism, ferroelectricity and ferroelasticity are observed [1-3]. Among all the multiferroic materials studied till now, ABO_3 typeperovskite structure $BiFeO_3$ (BFO) is environmental friendly material [4]. BFO shows ferroelectricity with a high curie temperature, Tc ~ 1103 K and with G- type antiferromagnetic Neel temperature T_N ~ 643 K [5, 6]. BFO has a distorted rhombohedral structure with space group R3c. BFO is not only used for developing novel storage media and spintronics devices, but also finds potential ability to couple electric and magnetic polarizations (magneto-electric effect). BFO finds applications as magnetoelectric sensor devices, multiple state memories, transducers, ferromagnetic resonance devices and ultrafast optoelectric device due to its small energy gap [7-9]. However, large leakage current, high dielectric loss, low remnant polarization, low electric resistivity and inhomogeneous magnetic spin structure are the drawbacks of BFO still to overcome in device applications [10, 11].

Several researchers have tried to improve multiferroic properties of BFO by substituting rare-earth metals and transition metals in A and B sites [12]. The importance of the phonons behavior in BFO, which is only multiferroic material, is recently reported in single crystal BFO, epitaxial BFO films and polycrystalline BFO sample [13-15] establishing the importance of phonon-spin coupling. Kothari *et al.,* [13] reported Raman spectra of polycrystalline BFO sample. Fukumura *et al.*, [14] reported all 13 Raman modes for single crystal BFO sample and pointed out discrepancy of Haumont *et al.*, [15] results. Haumont *et al.*, reported

* Corresponding author
E-mail address: kvkphd@gmail.com (K. V. Kumar)

anomalies in the phonon spectra of BFO sample near the Neel temperature (T_N). A Lahmar *et al*., have reported ferroelectricity, improved dielectric properties and the structural transition in $BiFeO_3$- $LaMnO_3$ solid solution thin film [16]. In present work, we report Mn doped BFO powders synthesized using citric acid sol-gel method and its structural and dielectrical properties.

2. Experimental

The polycrystalline $Bi_{1-x}Mn_xFeO_3$(x=0.0, 0.1, 0.2, 0.3) were synthesized by sol-gel method [17-20]. Stoichiometric amounts of the A. R. grade bismuth (III) nitrate pentahydrate ($Bi(NO_3)_3.5H_2O$), manganese chloride tetrahydrate ($MnCl_2.4H_2O$), iron (III) nitrate nonahydrate ($Fe(NO_3)_3.9H_2O$) and citric acid monohydrate ($C_6H_8O_7.H_2O$), were used as starting materials. During synthesis, an excess of ≈5wt.% Bi was added to compensate bismuth oxide loss during the thermal treatment. The mixture was stirred in a magnetic stirrer for 1hr till clear solution was obtained, with simultaneous drop by drop addition of ammonia solution added for neutralization of mixer. The entire process is explained elsewhere [19]. Then the prepared powder samples were annealed at 600°C for 5 hours.

The Raman measurements on BMFO ($Bi_{1-x}Mn_xFeO_3$, x=0.0, 0.1, 0.2, 0.3) samples were carried out using 488 nm excitation source by Jobin-Youn Horiba Labram (LABRAM-HR) Spectrometer equipment with a peltier cooled CCD detector. The Raman spectra were recorded in the range from 50 to 700 cm^{-1} with a resolution of 1cm^{-1}.

Electrical properties were measured using computer controlled a high precision electrometer (Radiant Technologies Inc.). Leakage current characteristics were acquired with a soak time of 100 ms and measure time 300 ms at 50 V. Dielectric properties were measured as a function of frequency (100 Hz to 1MHz) over a temperature range (room temperature to 500°C) using a precision impedance analyzer. (Nova Control, Alpha-high performance frequency analyzer).

3. Results and Discussions

Raman spectroscopy is sensitive to atomic displacements [21]. The Raman active modes of the rhombohedral $BiFeO_3$ with 3Rc structure at room temperature have been predicted using group theory were 13 activephonon modes $\Gamma_{Raman}= 4A_1+9E$. Where, A_1 modes are polarized along z-axis and E modes in x-y plane [13].

The A_1 modes are associated with Fe ions and E modes are associated with Bi ions [22]. Singh *et al*., reported 10 active modes for BFO epitaxial thin film with R3c structure including A_1^{-1}, A_1^{-2} and A_1^{-3} modes at 136, 168 and 211 cm^{-1} respectively, with strong intensity, A_1^{-4} mode at 425 cm^{-1} with quite weak intensity and six E modes at 275, 333, 365, 456, 549 and 597 cm^{-1} with medium intensity [23]. Kothari *et al*., reported 13 Raman active modes for polycrystalline BFO sample. The observed peaks were measured in both parallel and crossed polarization configurations. A_1 modes show decrease in intensity in the crossed polarization configuration as expected by polarization selection rules [13].

In our samples, all 13 of peaks of the rhombohedral $BiFeO_3$ with 3Rc structure due to $4A_1$ + 9E phonon active modes were observed at room temperature as shown in Figure 1. The observed and reported Raman peak position of BFO is illustrated in Table 1. The observed data for BFO is in agreement with that of Kothari*et al*., [13]. Raman scattering data clearly shows four high intensity peaks at 128 cm^{-1}, 166 cm^{-1}, 211cm^{-1} and 470 cm^{-1} corresponding to A modes. A shift was observed in A modes (A_1^{-1}, A_1^{-2} and A_1^{-4} and three E modes) towards higher wave number for BMFO (x= 0.1, 0.2, 0.3) with increasing Mn substitution, the intensities of A_1^{-2}, A_1^{-3}, A_1^{-4} and E modes decrease and the peaks are broadened.

Table 1. Comparison of Raman mode positions (cm^{-1}) the present study with the literature of BFO.

Raman modes	Kothari *et al. [13]*	Singh *et al. [43]*	Fukumura *et al. [14]*	BFO Present study
A_1^{-1}(cm^{-1})	135	136	126	128.8
A_1^{-2}(cm^{-1})	167	168	165	166
A_1^{-3}(cm^{-1})	218	211	213	211
A_1^{-4}(cm^{-1})	430	425	425	470
E(cm^{-1})	71	—	111.7	78
E(cm^{-1})	98	—	259.5	93
E(cm^{-1})	255	275	—	246
E(cm^{-1})	283	335	339.6	276
E(cm^{-1})	351	365	366.9	357
E(cm^{-1})	321	—	473.3	315
E(cm^{-1})	467	456	599.6	475
E(cm^{-1})	526	549	—	523
E(cm^{-1})	598	597	—	597

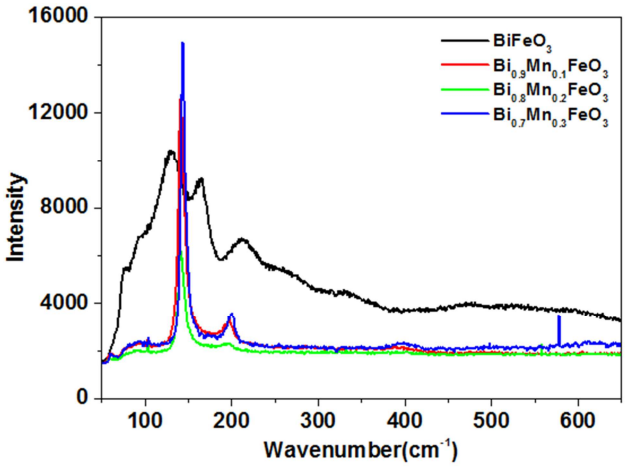

Figure 1. Raman spectrum of $Bi_{1-x}Mn_xFeO_3$ (x=0.0, 0.1, 0.2, 0.3).

The higher frequency shift may be due to substitution of light mass Mn^{2+} ions for heavier Bi^{3+} ions. This reduces significantly the average mass of A-site, as the frequency of the phonon mode inversely proportional to the reduced mass. It is observed that, the frequency of Raman modes are dependent on ionic mass, force constant and Bi-O bonding [13, 21, 24].

The A_1 (1 LO) and A_1 (2 LO) phonon modes attributed to Bi-O bond vibrations shows neither hardening nor softening after Mn incorporation. It is found that the intensity of A_1 (2 LO) mode decreases with increasing Mn content, indicating the tendency of a transition from rhombohedral to tetragonal phase [25]. As the Mn content increases from 0.1 to 0.3 for x, the A_1^{-1} mode shifts to higher frequency indicating the existence of tetragonal phase and is observed in all Mn doped BFO samples. Hence, these two aspects illustrate that Mn ions affect BFO crystalline symmetry in the samples. Furthermore, Mn doping causes substantial structural transition from rhombohedral to tetragonal phase, which is in agreement with XRD analysis [20].

Frequency dependent dielectric analysis for Mn doped BFO samples were performed at room temperature. Figure 2 shows the dielectric constant properties of BMFO ($0.00 \leq x \leq 0.3$) samples with the applied frequency of 100 Hz to 1MHz at room temperature. Dielectric constant was observed to decrease gradually with the increase in frequency and almost merge at higher frequencies (above 10 kHz). At low temperature, dipole relaxation may be responsible for observed dispersion in dielectric constant. During sintering, the non-uniform distribution of oxygen ions will take place at the grain boundaries. This might contribute for interfacial polarization at lower frequencies. Near high frequencies other polarizations such as dipolar, ionic, electronic may also contribute for observing dielectric constant [26]. With the increase in applied frequency, the polarization causes the reduction of field inside the medium; therefore the decrease in the dielectric constant is observed [27]. The change in the dielectric constant verses frequency is based on the space charge polarization due to the occurrence of high conductivity grains disconnected from low conductivity grain boundaries in the dielectric medium [28].

The association of space charge carriers in the dielectric material will try to line up parallel to the alternating field with a finite time. If the field reversal frequency increases, at a certain point the space charge carriers will not respond and lags in the direction of applied field [29]. Therefore, the decrease in the dielectric constant is observed. It is observed that, with the increase of Fe ions at the octahedral sites, the charge transfer between Fe^{2+} and Fe^{3+} ions takes place therefore high dielectric values are observed in many materials [30]. According to the Koops model, the dispersion observed in the dielectric constant is due to the response of electrons with the applied electric field under certain time constraint with the alternating applied field [31].

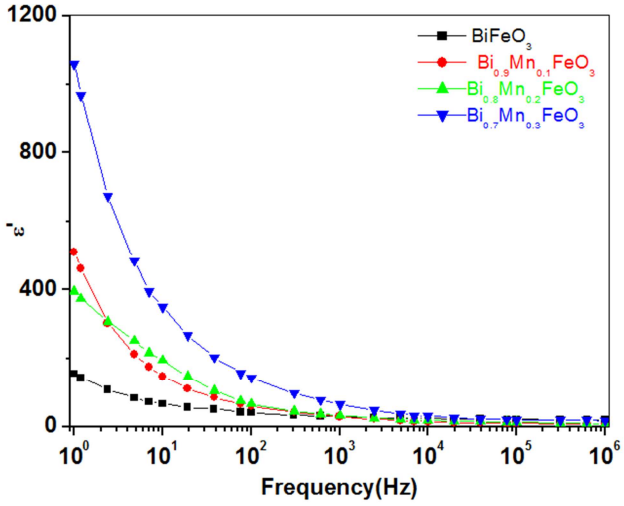

Figure 2. Variation of real part of permittivity (ε') with frequency of $Bi_{1-x}Mn_xFeO_3$ (x=0.0, 0.1, 0.2, 0.3) at room temperature.

Figure 3 shows the imaginary part of the dielectric constant of BMFO ($0.00 \leq x \leq 0.3$) samples measured with the applied frequency. These results are similar to the dielectric properties as explained by Smith and Wijn [32]. There exists an inverse relationship with the applied field between the complex dielectric permittivity towards ac conductivity ratios [32]. It has been predicted from these graphs that, the values of '€r' and tanδ decreases regularly with increasing frequency. Low frequency dispersion behavior in the dielectric constant and dielectric loss indicates the presence of dc conductivity in the samples. It was found that dielectric constant and dielectric loss reduces with increasing frequency and is attributed to the dipole relaxation. A high frequency Fe^{2+} - Fe^{3+} dipoles are not able to follow the field reversal. At low frequency the observed large dielectric constant values may be attributed to the interfacial

polarization and grain boundary effects. Materials possessing high conductivity values usually have higher dielectric losses or vice versa [33, 34].

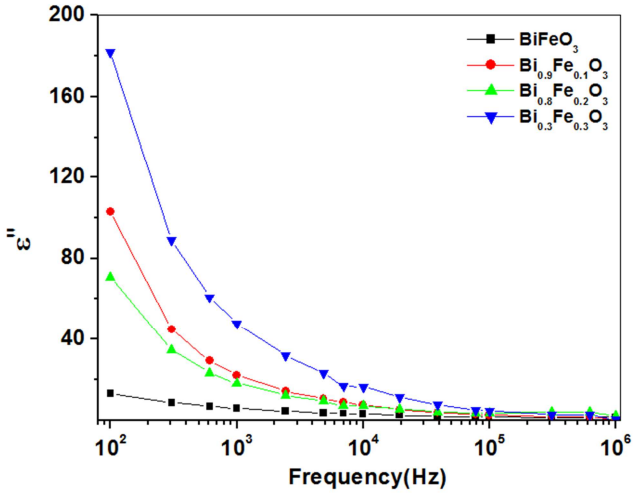

Figure 3. Variation of imaginary part of permittivity (ε") with frequency for $Bi_{1-x}Mn_xFeO_3$ (x = 0.0, 0.1, 0.2, 0.3) at room temperature.

Figure 4 indicates the variation in dielectric loss tangent of BMFO (x = 0.0, 0.1, 0.2, 0.3) with frequency. The variation in the dielectric loss (tanδ) in the samples may be due to several reasons such as chemical composition, structural homogeneity, stoichiometry, sintering temperature etc. [35-37].

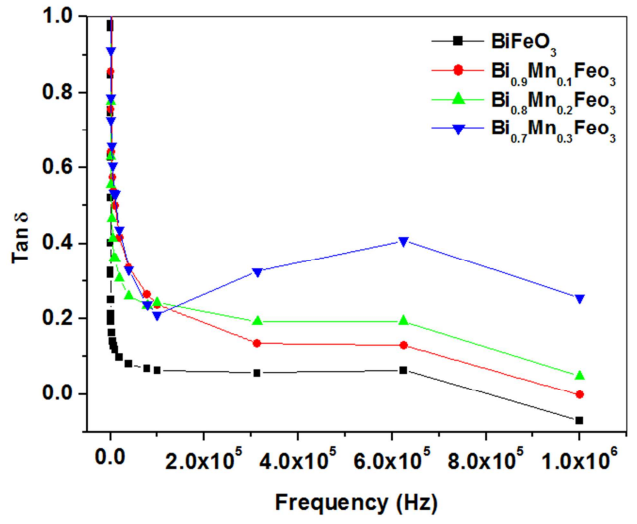

Figure 4. Variation of dielectric loss (tan δ) with frequency for $Bi_{1-x}Mn_xFeO_3$ (x=0.0, 0.1, 0.2, 0.3) at room temperature.

Based on the Maxwell–Wagner theory, it is known that dielectric properties έ and tanδ are inversely proportional to the frequency [36, 38, 39]. Materials having low dielectric losses are used in the low core loss and energy dissipation systems [37]. Dielectric constant for Mn doped BFO samples were observed to increase from 175 for BFO to 1175 for 0.2 sample. The dielectric loss remains in the range 0.1 - 0.3 for all the remaining samples. The observed enhancement in the dielectric constant for Mn doped BFO samples is predicted based on the enhanced interfacial polarization arising due to the large volume fraction of grain boundary.

At room temperature, for all the samples, it is observed that they exhibit moderately low dielectric losses. Figures 5–8 show the dielectric constant verses frequency for Mn doped BFO samples measured at different temperatures. As the Mn doping concentration increased, permittivity data was observed to improve significantly. A small anomaly in the dielectric data was observed for x = 0.1 and 0.3 around 380°C which significantly disappeared for x = 0.2 sample. After this temperature, all the samples showed stable behavior. The dielectric loss was observed to increase with change in temperature up to 350°C and thereafter it raised sharply due to higher thermal conductivity.

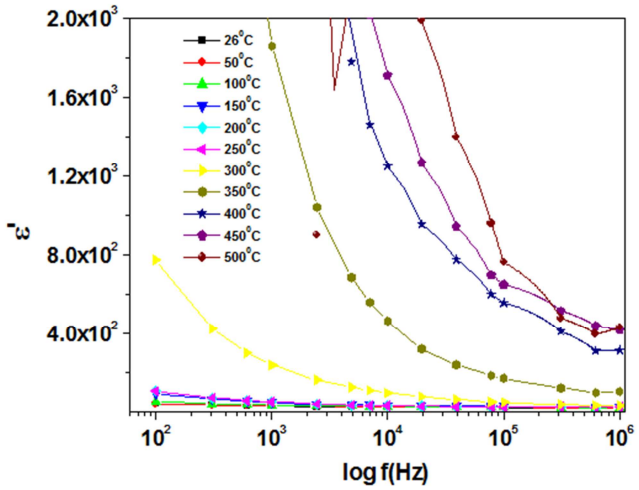

Figure 5. Variation of dielectric constant (ε') with log (frequency) at various temperatures for pure BFO.

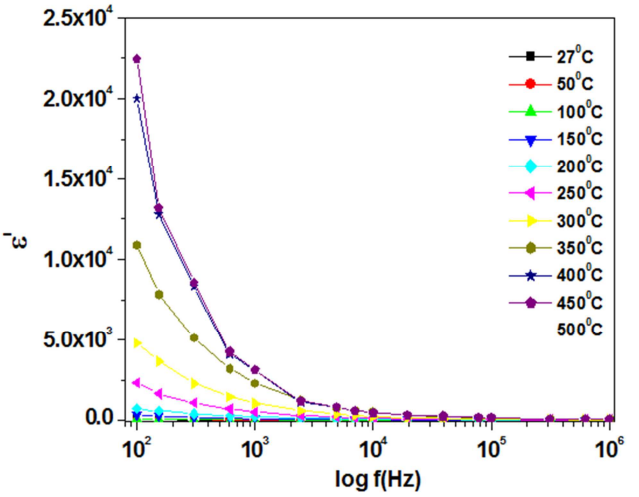

Figure 6. Variation of real part of dielectric constant (ε') with log (frequency) at various temperatures for $Bi_{0.9}Mn_{0.1}FeO_3$.

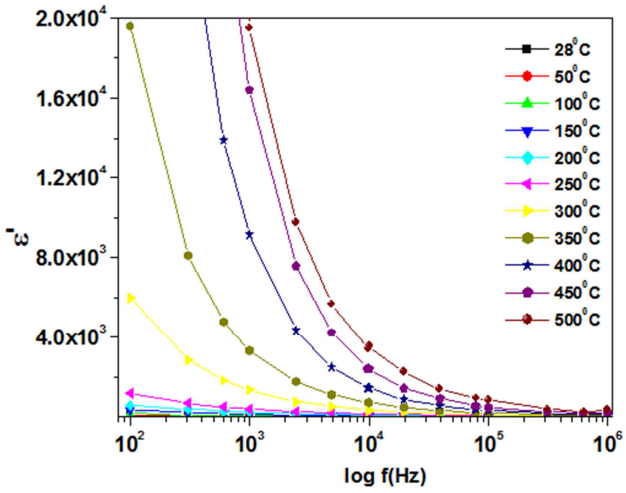

Figure 7. Variation of real part of dielectric constant (ε') with log (frequency) at various temperatures for $Bi_{0.8}Mn_{0.2}FeO_3$.

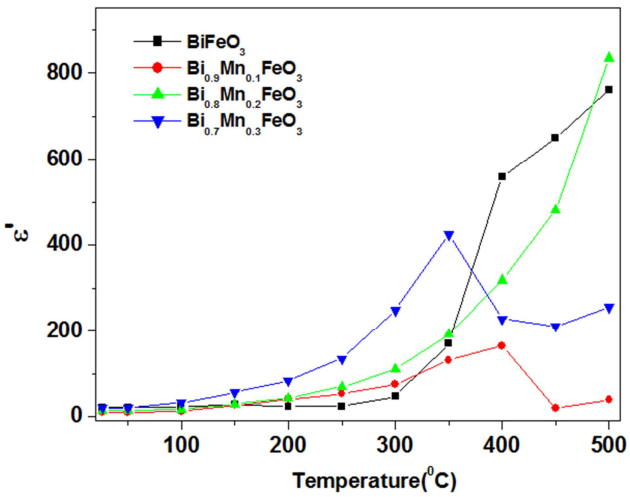

Figure 9. Variation of dielectric constant (ε') with temperature for $Bi_{1-x}Mn_xFeO_3$ (x=0.0, 0.1, 0.2, 0.3) at 100 KHz.

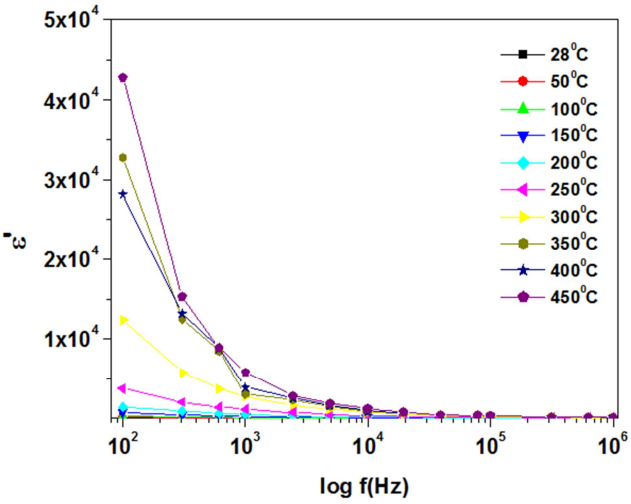

Figure 8. Variation of real part of dielectric constant (ε') with log (frequency (Hz)) at various temperatures for $Bi_{0.7}Mn_{0.3}FeO_3$.

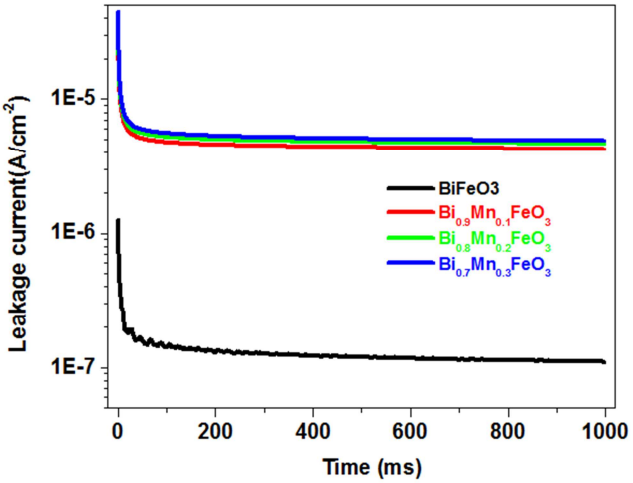

Figure 10. Variation of leakage current density with time at room temperature for $Bi_{1-x}Mn_xFeO_3$ (x= 0.0, 0.1, 0.2, 0.3) at 50V.

Figure 9 shows the variation of dielectric constant (ε) with temperature for Mn doped BFO ($0.00 \leq x \leq 0.3$) samples measured at frequency 100 kHz. All the samples were frequency dependent as they exhibit broad dielectric permittivity peaks. Curie-Weis law is used to describe the dielectric dispersion observed in the Mn doped BFO samples [40]. In dielectric materials the oxygen vacancies plays quite important role than the dopants. It is very well known that in dielectric materials, oxygen vacancies contribute for low dielectric values [41, 42]. Compared to x = 0.1 or 0.3, the x = 0.2 sample showed lower oxygen vacancies and higher ε values.

Figure 10 depicts the leakage current density variation with time at room temperature measured with 50 V for the pure BFO and Mn doped BFO samples. From the graphs, it is observed that the leakage current increased with increasing the Mn doping compared to pure BFO sample.

Leakage current refers to the gradual loss in the energy from a charged material such as a capacitor. This may be caused when the capacitors are attached to electronic components, like diodes or transistors. These components even conduct under switch-off condition also. During the switch-off conditions, the currents flows through the devices and discharges slowly through the capacitor. Undesired imperfection in some dielectric materials could also contribute for leakage currents in capacitors. This phenomenon is called as *dielectric leakage*. When the dielectric material is not perfect insulator, it will have small amount of non-zero conductivity which allows the *leakage current* to discharge slowly.

The current instead of flowing in a proper circuit, it takes alternate path through which the current leaks from the electronic circuit. This is also considered as leakage current. This kind of leakage current is undesirable in electronic circuits. Because, when the current flows from the alternate

paths, it will damage the electronic devices in the form of fires, electrocution and RF noise.

Leakage current transfers unwanted energy from circuit to circuit and from component to component. Therefore in electronic assemblies, they make the circuit's disable, standby, sleep mode etc. These devices may draw small amount of current such as one or two microamperes when they are in quiescent conditions when compared to huge milliamperes when in full operations. A leakage current is one of the important factors which is becoming significant concept in device manufacturing. Because, they produce undesirable and significant affects on the battery run time in consumer applications.

Enhanced leakage current in semiconductor could also result from the defects during fabrication and manufacturing process. Leakage current in general is measured in microamperes. Leakage current will vary according to operating temperature conditions and those properties should be examined carefully when using in practical applications.

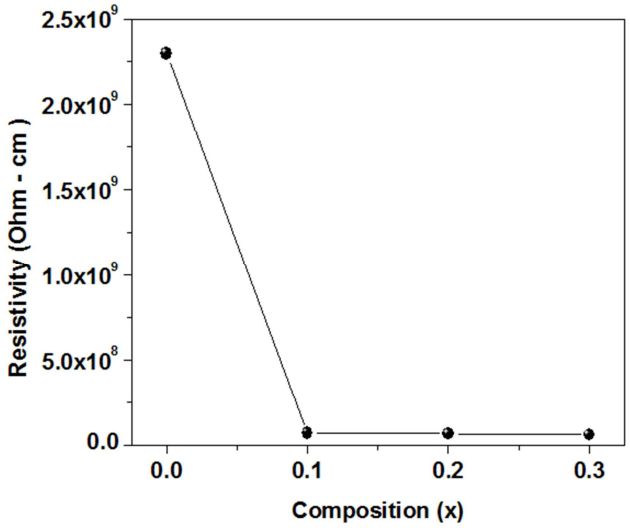

Figure 11. Variation of Resistivity with composition at room temperature for $Bi_{1-x}Mn_xFeO_3$ (x= 0.0, 0.1, 0.2, 0.3).

Figure 11 shows the resistivity versuss composition for pure BFO and Mn doped BFO samples. It is observed that, the resistivity is drastically decreased for Mn doped BFO samples when compared to pure BFO sample. This also reflects in the leakage current density graph. The leakage current increases with increasing Mn doping in BFO compared to pure BFO sample.

From Figure 10 and 11, one can clearly observe that these samples have very small leakage currents. The leakage current values are in good agreement with the BFO samples prepared by other techniques [44-48].

However, in Mn doped BFO samples the leakage current could be understood by relating to grain size distribution. Grains having different sizes, shapes, structures, their boundary conditions are considered to play a prominent role most of the time for contributing the leakage current. Lubomirsky et al. [47], investigated the space–charge effect modelling in nanostructured materials and concluded that, contacts between different sized grains may lead to energy exchange between the grains, called as hetero size charging. This will fundamentally influence the conductivity among the smaller grains as they generally conduct at lower voltages [47].

Figure 12 gives the variation of current density with electric field for all Mn doped BFO samples. It is observed that the current density values are more for the Mn doped BFO samples when compared with pure BFO sample. The current density values were observed to decrease with increasing the positive applied field. While it increased with the negative applied field in all samples. But the current density values for all the Mn concentrations remain same. This may be due to dipolar polarization which contributes to the current density. However, the increase of current density with increase of Mn concentration is less significant. But doping of Mn in BFO contributes large variation of current density in BFO sample [49-53].

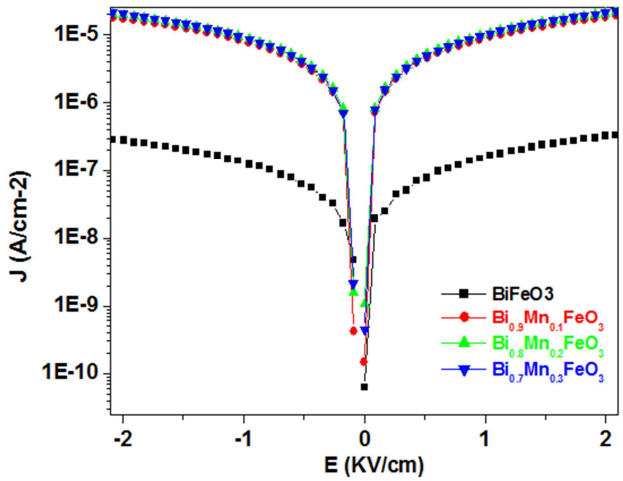

Figure 12. Variation of current density (J) with electric field (E) for $Bi_{1-x}Mn_xFeO_3$ (x= 0.0, 0.1, 0.2, 0.3) at room temperature.

4. Conclusions

Pure and Mn doped BFO samples have been synthesized using sol-gel method. Raman analysis confirmed rhombohedral (3Rc) BFO structure. In dielectric studies, dielectric constant (both ε' and ε") and dielectric loss decreased with increasing frequency (100Hz to 1MHz) at room temperature. Dielectric constant and loss dispersion increased with increasing temperature. Leakage current density was observed to increase with Mn doping concentration.

References

[1] B Bhushan, A Basumallick, S K Bandopadhyay, N Y Vasanthacharya and D Das, J. Phys. D. Appl. Phys., 42, 065004 (2009).

[2] Mfiebig, TLottermoser, D Frohlich, A V Goltsev and R VPisarev, Nature, 419, 818 (2002).

[3] WEerenstein, N D Mathur and J F Scott, Nature, 442, 759 (2006).

[4] Y Satio, H Takao, T Tani, TNonoyama, K Takatori, T Homma, T Nagaya and M Nakamura, Nature, 432, 84 (2004).

[5] M MKumar, V R Palkar, K Srinivas and S V Suryanarayana, Appl. Phys. Lett., 76, 2764 (2000).

[6] J V Rivera and H Schmid, Ferroelectrics, 204, 23 (1997).

[7] M Fiebig, J. Phys. D. Appl. Phys., 38, R123 (2005).

[8] N. A. Hill, J. Phys. Chem., B104, 6694 (2000).

[9] K. Takahashi, N. Kida and M. Tonouchi, Phys. Rev. Lett., 96, 117402 (2006).

[10] Zuci Quan, wei Liu, Hao Hu, Sheng Xu, Bobby Sebo, Guojia Fang, Meiya Li, and Xingzhoong Zhao, J. Appl. Phys., 104, 084106, (2008).

[11] C. Ederer and N. A. Spaldin, Phys. Rev. B., 71, 060401, (2005).

[12] X. Qi, J. Dho, R. Tomov, M. G. Blamire, J. L. Mac-Manus-Drisol, Appl. Phys. Lett., 86, 062903 (2005).

[13] Deepti Kothari, V. Raghavendra Reddy, V. G. sathe, Ajay Gupta, A. Banerjee, A. M. Awasthi, J. Magn. Magn. Mater., 320, 548 (2008).

[14] H. Fukumura, H. Harima, K. Kisoda, M. Tamada, Y. Noguchi, M. Miyayama, J. Magn. Magn. Mater., 310, e367 (2007).

[15] R. Haumont, J. Kreisel, P. Bouvier, F. Hippert, Phys. Rev. B., 73, 132101, (2006).

[16] A. Lahmar, S. Habouti, C. H. Solterbeck, M. Es-Souni and B. Elouadi, J. Appl. Phys., 105, 014111 (2009).

[17] T Y Kim, N H Hong, T Sugawara, A T Raghavender, and M Kurisu, J. Phys: Cond. Mat, 25, 206003 (2013).

[18] A. T. Raghavender, N. H. Hong, C. Park, M.-H. Jung, K. J. Lee, and D. Lee, Materials Lett., 65, 2786 (2011).

[19] A. T. Raghavender and N. H. Hong, J. Magnetics, 16, 19 (2011).

[20] V. Srinivas, A. T. Raghavender, and K. Vijaya Kumar, 2016, 4835328, (2016).

[21] Pawan Kumar, Manoranjan Kar, Materials Chem. and Phys., 148, 968 (2014).

[22] Dinesh varshney, Ashwini Kumar, Kavitha Verma, Journal of Alloys and Compounds 509, 8421 (2011).

[23] S K Singh, H Ishiwara and maruyama, Appl. Phys. Lett. 88, 262908 (2006).

[24] Pragna Pandit, S Satapathy, Poorva Sharma, P K Gupta, S M Yusuf and V G Sathe, Bulletin of Materials Science 34, 899 (2011).

[25] Ji-Zhou Huang, Yang Shen, Ming Li, and Ce-Wen Nan, J. Appl. Phys, 10, 094106, (2011).

[26] . S. B. Narang, I. S. Hudiara, J. Cer. Processing Research 7, 113, (2006).

[27] S. F. Mansour, Egyptian Journal of Solids 2, 263,(2005).

[28] M. Chanda, Science of Engineering Materials, The Machmillan Company of India Ltd., New Delhi 3 (1980).

[29] A. M. Shaikh, S. S. Bellad, B. K. Chougule, J. Magn. Magn. Mater., 195, 384 (1999).

[30] M. J. Iqbal, M. N. Ashiq, P. Hernandez-Gomez, J. M. Munoz, J. Magn. Magn. Mater., 320, 881 (2008).

[31] M. Anis-ur-Rehman, G. Asghar, J. Alloys and Compounds 509, 435 (2011).

[32] G. F. M. Pires Júnior, H. O. Rodrigues, J. S. Almeida, E. O. Sancho, J. C. Góes, M. M. Costa, J. C. Denardin, A. S. B. Sombra, J. Alloys and Compounds, 493, 326 (2010).

[33] M. N. Ashiq, M. J. Iqbal, I. H. Gul, J. Alloys and Compounds 487, 341 (2009).

[34] I. H. Gul, A. Maqsood, J. Alloys and Compounds, 465, 227 (2008).

[35] M. N. Ashiq, M. Javed Iqbal, I. Hussain Gul, J. Magn. Magn. Mater., 323, 259 (2011).

[36] R. Peelamedu, C. Grimes, D. Agrawal, R. Roy, J. Materials Research, 18, 2292 (2003).

[37] M. Javed Iqbal, M. Naeem Ashiq, I. Hussain Gul, J. Magn. Magn. Mater., 322, 1720 (2010).

[38] Manoj Kumar, K. L Yadav, Appl. Phys. Lett. 91, 242901, (2007).

[39] A. Molak, D. K. Mahato, A. Z. Szeremeta, Progress in Crystal Growth and Characterization of Materials, 64, 1 (2018).

[40] K. Uchino, S. Nomura, Ferroelectrics. Lett., 44, 55 (1982).

[41] W. Eerenstein, F. D. Morrison, J. Dho, M. G. Blamire, J. F. Scott, and N. D. Mathur, Science, 307, 1203 (2005).

[42] X. Qi, Appl. Phys. Lett., 86, 062903, (2005).

[43] M. K. Singh, H. M. jang, S. Ryu, M. H. Jo, Appl. Phys. Lett., 88, 42907 (2006).

[44] V R Reddy, Deepti Kothari, Sanjay Kumar Upadhyay, Ajay Gupta, N. Chauhan, and A. M. Awasthi, Ceramics International 40, 4247 (2014).

[45] Pabst, Gary W., Lane W. Martin, Ying-Hao Chu, and R. Ramesh, Appl. Phys. Lett., 90, 2902 (2007).

[46] Khan, A Mikael, P C Tim, and J B Andrew, Appl. Phys. Lett., 92, 072908, (2008).

[47] Lubomirsky, Igor, Juergen Fleig, and Joachim Maier, J. Appl. Phys., 92, 6819, (2002).

[48] Wang, Can, Mitsue Takahashi, Hidetoshi Fujino, Xia Zhao, EijiKume, Takeshi Horiuchi, and Shigeki Sakai, J. Appl. Phys., 99, 54104 (2006).

[49] R. G. Lerner, G. L. Trigg, Encyclopaedia of Physics (2nd Edition), (VHC publishers, 1991, ISBN (Verlagsgesellschaft)) 3-527-26954-1.

[50] Martin, Richard M., Electronic structure: basic theory and practical methods. (Cambrisdge university press, 2004).

[51] A. Altland and B. Simons, Condensed Matter Field Theory, (Cambridge University Press, 2010).

[52] Yun, Kwi Young, Minoru Noda, Masanori Okuyama, Hiromasa Saeki, Hitoshi Tabata, and Keisuke Saito, J. Appl. Phys., 96, 3399 (2004).

[53] Wang, Can, Mitsue Takahashi, Hidetoshi Fujino, Xia Zhao, EijiKume, Takeshi Horiuchi, and Shigeki Sakai, J. Appl. Phys., 99, 54104 (2006).